IOP Publishing New J. Phys. 25 (2023) 043025 https://doi.org/10.1088/1367-2630/accec3

New Journal of Physics
The open access journal at the forefront of physics

Deutsche Physikalische Gesellschaft DPG
IOP Institute of Physics

Published in partnership with: Deutsche Physikalische Gesellschaft and the Institute of Physics

OPEN ACCESS

RECEIVED
13 October 2022

REVISED
31 March 2023

ACCEPTED FOR PUBLICATION
20 April 2023

PUBLISHED
28 April 2023

PAPER

Defect induced nonequilibrium quantum dynamics in an interacting Bose–Hubbard flux ladder

Yue Jian[1,2], Ai-Xia Zhang[1], Xin Qiao[1], Jun-Cheng Liang[1], Zi-Fa Yu[1] and Ju-Kui Xue[1,*]

[1] College of Physics and Electronic Engineering, Northwest Normal University, Lanzhou 730070, People's Republic of China
[2] Department of Basic Sciences, Lanzhou Institute of Technology, Lanzhou 730050, People's Republic of China
* Author to whom any correspondence should be addressed.

E-mail: xuejk@nwnu.edu.cn

Keywords: nonequilibrium quantum dynamics, interacting Bose–Hubbard flux ladders, dynamical quantum phase transition

Abstract

The interacting Bose–Hubbard flux ladder provides an ideal model to probe novel quantum phenomena of many-body systems. Here, we report on the first direct observation of dynamical quantum phase transition (DQPT) in interacting Bose–Hubbard flux ladder induced by defect perturbation, which provides a new scheme for experimental design and manipulation of the DQPT in ultracold atomic system. Under the mean-field approximation, DQPT is identified by resolving the order parameter and the temporal evolution of patterns of atomic density distributions and local current configurations of the system. The threshold for occurrence of DQPT is obtained analytical and the physical mechanism of DQPT is revealed explicitly. Periodic appearance and annihilation of dynamical vortex and the manifestation of symmetry restoration after perturbation from broken-symmetry phase are observed. A thorough connection among the order parameter dynamics, the underlying ground state phase transition and nonequilibrium dynamics is established in real time and real space for the first time. Interestingly, by quenching the defect, the underlying ground state phases are captured, which provides a feasible dynamical measurement scheme for the observation of the underlying ground state phase which is challenging to reach experimentally.

1. Introduction

Nonequilibrium quantum many-body dynamics is of great significance in quantum physics and statistical mechanics [1, 2], and may provide a new way to realize quantum manipulation and quantum technology. Due to deepened theoretical understanding and experimental technology advances in recent years, nonequilibrium quantum dynamics has been developed rapidly [3–9]. Dynamical quantum phase transition (DQPT) is a central issue in this field [3, 4], which extends the concept of phase transitions and thus universality to the nonequilibrium regime, and has been demonstrated in quench experiments with cold atoms in optical lattices [7, 9–11] and cavities [12], trapped ions [13, 14], and with superconducting qubits [15]. Quantum system coupled to a dissipative environment also offers a unique testing ground for exploring nonequilibrium dynamics, and the dynamical transition between coherent oscillatory and overdamped dynamics has been received much attention [16–19]. One notable phenomena in DQPT is nonanalyticity characterized by a nonequilibrium order parameter after a quantum quench [12, 20–22] or by the appearance of critical times when the return probability becomes nonanalytic [13, 23]. In particular, a DQPT can trigger nontrivial dynamics that allows one to define new concepts of nonequilibrium criticality, to establish a connection between DQPT and the underlying equilibrium state phase transition, and to identify and control the ground state phase which is challenging to reach experimentally [20, 24–27]. Substantial progress has been made in this field recently, from identifying dynamical order parameters [28–30], or scaling and universality [31, 32], to the first experimental observations [13], and further applied to the study of entanglement dynamics, quantum speed limits and mixed states [33–35].

Nevertheless, understanding general properties of DQPT remains a major challenge [3, 32, 36–39] and many key issues need to be settled, including identifying experimental accessible observables whose dynamics are linked to DQPT, resolving under what circumstances DQPT occur. Particularly, most studies on DQPT are restricted to one dimension, investigation of DQPT in two-dimensional systems is highly challenging. Furthermore, the connection of DQPT with order parameter dynamics and equilibrium phase transitions remains elusive for nonintegrable models [3, 40–43]. Hence, revealing explicit relationship among the order parameter dynamics, the underlying ground state phase and nonequilibrium dynamics is still an open topic, which is even more challenging for systems in higher dimensions.

Combing the orbital magnetic field and lattice coupling effects in low dimensional system, the Bose–Hubbard flux ladder [44] provides an ideal model to simulate two-dimensional topological physics and probe novel quantum phenomena of many-body systems, e.g. exploring the physics of the edges of Chern insulators and Hall effect, realizing spin–orbit (SO) coupling and topological superfluid phase [44–47]. The unique energy spectrum structure of the system results in rich quantum phases [48–50]. The lowest energy band can be parabolic with single minimum at $k=0$ (where the system is in Meissner phase with $k=0$) or double-well with two symmetric minima at $k=\pm k_0$ (where the system is in vortex phase-a superposition of the two degenerate states at $k=\pm k_0$), here k is the quasimomentum of the atoms. Accordingly, ground states breaking discrete symmetry, such as charge-density-wave and vortex-lattice [51, 52], are also found. Interestingly, due to the atomic interaction, there is a novel ground state phase-the biased ladder (BL) phase, which is a double degenerate quantum state, and bosons can condense in a single momentum state $k=k_0$ or $k=-k_0$ [52–54]. This novel ground state phase of the interacting Bose–Hubbard flux ladder provides superior conditions for the generation of multiple equilibrium states and becomes an ideal platform for the study of nonequilibrium quantum dynamics. Stability and superfluidity, chiral Bloch–Zener dynamics, Stückelberg interference, critical slowing down of the collective modes, and dynamical supersolidlike phases are presented [54–63]. However, which nontrivial nonequilibrium quantum dynamics can be excited by applying an external perturbation to resonantly couple the two degenerate quantum states in Bose–Hubbard flux ladder has never been studied. Correspondingly, the DQPT excited by the perturbation and the relationship between the nonequilibrium dynamics and the underlying ground state phases in the system are still open subjects.

Here, defining polarizability as an observable order parameter, we report on the first direct observation of DQPT in interacting Bose–Hubbard flux ladder induced by lattice defect perturbation and identified by resolving the order parameter and the temporal evolution of patterns of atomic density distributions and local current configurations. DQPT is robust against weak defect perturbation of the underlying Hamiltonian. A new scheme, i.e. defect perturbation, for exciting and manipulating of DQPT in ultracold atomic system is established, which is distinct from the one currently used, i.e. quantum quench. The threshold for occurrence of DQPT is obtained analytical and the physical mechanism of DQPT is revealed explicitly. The competition between the atomic interaction and the defect results in DQPT, which can be manipulated by magnetic field and rung-to-leg coupling ratio. When the defect perturbation is dominant, the two quantum states are resonantly coupled, DQPT is excited and periodic appearance and annihilation of dynamical vortex and the manifestation of symmetry restoration after perturbation from broken-symmetry phase are observed. A thorough connection among the order parameter dynamics, the underlying ground state phase transition and nonequilibrium dynamics is established in real time and real space for the first time. Interestingly, by quenching the defect, the underlying ground state phases are captured, which provides a feasible dynamical measurement scheme for the observation of the underlying ground state phase which is challenging to reach experimentally.

The paper is organized as follow. In section 2, the model of the interacting Bose–Hubbard flux ladder is established, and the three ground state phases are described. In section 3, through theoretical analysis, the nonequilibrium quantum dynamics of the system induced by single lattice defect perturbation is studied and its physical mechanism is elaborated. In section 4, the DQPT induced by the randomly distributed defects is discussed. In section 5, a brief summary is given.

2. The model and the ground state phase

The tight-binding Hamiltonian for the interacting Bose–Hubbard flux ladder with defect is given by [44, 53, 64–66]

$$\hat{H}=-\tilde{J}\sum_{j}(\mathrm{e}^{i\phi}\hat{a}_{j,L}\hat{a}^{\dagger}_{j+1,L}+\mathrm{e}^{-i\phi}\hat{a}_{j,R}\hat{a}^{\dagger}_{j+1,R}+h.c.)-\tilde{K}\sum_{j}(\hat{a}^{\dagger}_{j,L}\hat{a}_{j,R}+h.c.)+\frac{\tilde{g}}{2}\sum_{j,\sigma}|\hat{a}_{j,\sigma}|^4+\tilde{\epsilon}_j\sum_{j,\sigma}|\hat{a}_{j,\sigma}|^2, \quad (1)$$

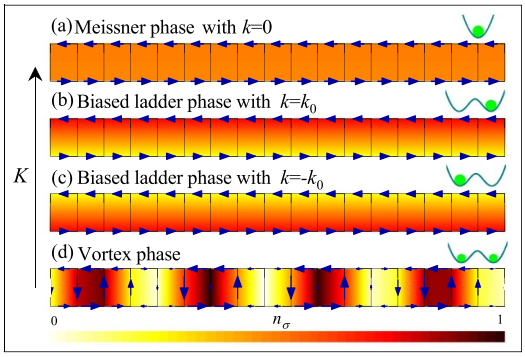

Figure 1. The schematic diagrams of the Meissner phase, the biased ladder phase and the vortex phase for the pure flux ladder.

where j refers to the jth site. $\hat{a}_{j,\sigma}$ and $\hat{a}^{\dagger}_{j,\sigma}$ are the bosonic annihilation and creation operators on site j along the leg of the ladder (σ stands for L or R). The hopping matrix elements along the legs and rungs of the ladder are $\tilde{J}$ and $\tilde{K}$, respectively. The magnetic flux per unit cell is ϕ, and the atomic interaction strength between arbitrary two atoms in a site is $\tilde{g}$. $h.c.$ stands for the conjugate term. $\tilde{\epsilon}_j$ is the strength of the defect, which can be localized or extended in space. The defect, i.e. weak random impurities or disorders (which can be parametric or additive, temporal or spatial), cannot be completely avoided in real system. Experimentally, defect can be introduced in ultracold gases in a controlled way by using optical potentials, especially can be controlled by laser speckles [67]. In addition to optical means, defected potential could also be created by using atomic mixtures [68] or inhomogeneous magnetic fields [69].

Under the mean-field approximation, ($\langle \hat{a}_{j,\sigma} \rangle = a_{j,\sigma}$), the tight-binding Hamiltonian (1) is given by

$$H = -\sum_{j}(\mathrm{e}^{i\phi}a_{j,L}a^{*}_{j+1,L} + \mathrm{e}^{-i\phi}a_{j,R}a^{*}_{j+1,R} + h.c.) - K\sum_{j}(a^{*}_{j,L}a_{j,R} + h.c.) + \frac{g}{2}\sum_{j,\sigma}|a_{j,\sigma}|^4 + \varepsilon_j\sum_{j,\sigma}|a_{j,\sigma}|^2, \quad (2)$$

where $K = \tilde{K}/\tilde{J}$, $g = \tilde{g}/\tilde{J}$ and $\epsilon_j = \tilde{\epsilon}_j/\tilde{J}$. The time is rescaled as $t \to [\hbar/\tilde{J}]t$. $a_{j,\sigma}$ is the probability amplitude of atoms on site j along the leg of the ladder and satisfies the normalization condition $\Sigma_j(|a_{j,L}|^2 + |a_{j,R}|^2) = 1$. The first, second and third terms of equation (2) correspond to the kinetic energy, the atomic interaction energy and the coupling energy caused by defect perturbation, respectively. Experimentally, this ladder system can be readily realized by combining effective magnetic fields with superlattice structures [44].

For the pure system, i.e. $\varepsilon_j = 0$, the ground state can be described by the two superimposed plane waves (the superimposed states) $a_{j,\sigma} = a_{\sigma+}\mathrm{e}^{ikj} + a_{\sigma-}\mathrm{e}^{-ikj}$, where $a_{\sigma\pm}$ and k are the amplitude and the quasimomentum. There are three ground state phases in the system (see figure 1): (1) the Meissner phase, which corresponds to the ground state with zero quasimomentum ($k = 0$) and can be described by the plane wave state, i.e. $a_{\sigma-} = 0$. In this phase, the atomic density along the ladder leg is uniform. The equal and opposite currents flow along the left and right legs, and there is no rung current. (2) the BL phase, which corresponds to the ground state with non-zero quasimomentum ($k = \pm k_0$), but only one of the two minima of the energy band is filled macroscopically, so it belongs to the single momentum state, and the system is also described by the plane wave state. In this phase, the atomic density is uniformly distributed along the ladder leg but different on the left and right legs. On the lower (higher) density leg, the fluid velocity is higher (lower), and the rung current is zero. The choice of ladder leg with higher (lower) density is arbitrary. (3) the vortex phase, which corresponding to the ground state with non-zero quasimomentum and is characterized by a macroscopic occupation of two momentum modes $k = \pm k_0$, so it is described by the superposition state. In this phase, the atomic density is modulated along the ladder and has rung current. The BL phase breaks the global U(1) symmetry and Z_2 reflection symmetry of the Hamiltonian equation (2) ($\varepsilon_j = 0$), and makes the system has the $k = \pm k_0$ two degenerate quantum states. Therefore, the dynamics of the system in this phase becomes particularly rich. In this work, we study the nonequilibrium quantum dynamics of the system induced by defect perturbation.

3. The dynamic quantum phase transition induced by single defect perturbation

3.1. Theoretical analysis

Preparing the system in $k = k_0$ state, we first focus on using single weak defect $\varepsilon_j = \varepsilon\delta_{j,\tilde{j}}$ as a perturbation to excite the resonant coupling between the two quantum states and study the nonequilibrium quantum dynamics of the system. In the pure system ($\varepsilon_j = 0$), the superposition of two opposite momentum states is

degenerate. The defect splits this degeneracy by coupling $k = k_0$ and $k = -k_0$ plane waves, which is very similar to the tunneling barrier in the double well potential and has left and right localized states. Therefore, the coupling of the two plane wave states can be described according to the effective Josephson Hamiltonian [70–72]. As long as the energy splitting caused by defect is much smaller than the energy gap between different quantum states, these Josephson regions can be retained. Under this limit, keeping only the transitions between the two ground states with $k = \pm k_0$, we can split all the excited modes into these two modes and neglect the overlapping of the two modes. In addition, the excitations of the higher-order terms, such as linear, quadratic, cubic and quartic terms, can be safely neglected due to the low occupancy of these terms. Then, we use the time-dependent superposition of the two quantum states as the condensate wave function to simulate the dynamics of the system:

$$a_{j,\sigma}(t) = \sqrt{n_{\sigma,+}(t)}\mathrm{e}^{i\varphi_{\sigma,+}(t)}\mathrm{e}^{ikj} + \sqrt{n_{\sigma,-}(t)}\mathrm{e}^{i\varphi_{\sigma,-}(t)}\mathrm{e}^{-ikj}. \tag{3}$$

Using $\sum_{j=1}^{N}\mathrm{e}^{2ikj} = 0$, here N is the total number of lattice sites, the effective Hamiltonian of the system is reduced to

$$\begin{aligned} H(t) = &\frac{1}{2}\cos(k-\phi)(n_{L,1}+n_{R,2}) \\ &+\frac{1}{2}\cos(k+\phi)(n_{R,1}+n_{L,2}) \\ &+\frac{K}{2}\left(\sqrt{n_{\mathrm{L},1}n_{\mathrm{R},1}}\cos\varphi_+ + \sqrt{n_{\mathrm{L},2}n_{\mathrm{R},2}}\cos\varphi_-\right) \\ &-\frac{g}{16}\left(n_{\mathrm{L},1}n_{\mathrm{L},2}+n_{\mathrm{R},1}n_{\mathrm{R},2}-n_{\mathrm{L},1}n_{\mathrm{R},1}-n_{\mathrm{L},2}n_{\mathrm{R},2}-n_{\mathrm{L},1}n_{\mathrm{R},2}-n_{\mathrm{R},1}n_{\mathrm{L},2}\right) \\ &-\frac{\varepsilon}{2N}\left(\sqrt{n_{\mathrm{L},1}n_{\mathrm{L},2}}\cos\varphi_{\mathrm{L}} + \sqrt{n_{\mathrm{R},1}n_{\mathrm{R},2}}\cos\varphi_{\mathrm{R}}\right). \end{aligned} \tag{4}$$

where $n_{\sigma,1} = 1 + (n_{\sigma,+} - n_{\sigma,-}) + (n_{\overline{\sigma},+} - n_{\overline{\sigma},-}) \pm 2(n_{\mathrm{L},+} - n_{\mathrm{R},+})$, $n_{\sigma,2} = 1 - 3(n_{\sigma,+} - n_{\sigma,-})$ $+(n_{\overline{\sigma},+} - n_{\overline{\sigma},-}) \pm 2(n_{\mathrm{L},+} - n_{\mathrm{R},+})$. $\varphi_\sigma = \varphi_{\sigma,+} - \varphi_{\sigma,-}$ is the phase difference between the two quantum states along the left and right ladder legs, $\varphi_i = \varphi_{\sigma,i} - \varphi_{\overline{\sigma},i}$ $(i = +,-)$ is the phase difference of ith quantum state between left and right ladder legs.

In order to characterize the nonequilibrium quantum dynamics of the system, we define $M_z(t) = \frac{i\Sigma_{n,\sigma}(a^\dagger_{n+1,\sigma}(t)a_{n,\sigma}(t) - h.c.)}{\Sigma_{n,\sigma}(a^\dagger_{n+1,\sigma}(0)a_{n,\sigma}(0) + h.c.)}$ as the order parameter to distinguish the quantum states. Using equation (3), we obtain

$$M_z(t) = \frac{\sum_\sigma(n_{\sigma,+}(t) - n_{\sigma,-}(t))}{\sum_\sigma(n_{\sigma,+}(0) + n_{\sigma,-}(0))}. \tag{5}$$

$M_z(t)$ is a quasi-polarizability and represents the normalized atomic density difference between the two degenerate quantum states. If the two degenerate states of the system are regarded as a kind of pseudospin, the model can be effectively analogized to the SO coupled system. Therefore, the pseudospin $M_\delta(t)$ of the system is defined by Pauli matrices acting on the pseudospin spanned by the two degenerate states with $\delta = x, y, z$. When $M_z(t) = 1$ or $M_z(t) = -1$, the condensate only fills in a macroscopic single quantum state, $k = k_0$ or $k = -k_0$, which is defined as the dynamical polarized state. When $M_z(t) = 0$, the condensate is in the superposition state with equal occupation of the two quantum states (the vortex state), $k = \pm k_0$, which is defined as the dynamical non-polarized state. The atomic interaction in the Hamiltonian also breaks the translational symmetry and can modulate the DQPT. The nontrivial competition between the atomic interaction and defect results in the DQPT. When the defect perturbation is dominant and the system is initially in single momentum state ($k = k_0$ or $k = -k_0$), the defect perturbation will induce the resonant coupling of the two quantum states, $M_z(t)$ will oscillate periodically with t between 1 and -1, $\langle M_z(t)\rangle = 0$, indicating that the system is in the dynamical non-polarized phase, DQPT takes place, here $\langle\ldots\rangle$ stands for a time average. $M_z(t)$ changes periodically with time. The time sample we take is large enough that the time average $\langle M_z(t)\rangle$ is not sensitive to time and reflects the intrinsic characteristic of the system. When the atomic interaction is dominant, it will inhibit the coupling of the two quantum states, $\langle M_z(t)\rangle > 0$, the system is in the dynamical polarized state (the single momentum state), and the DQPT is inhibited. This phenomenon reflects the nontrivial interaction effect on the transitions between many-particle states and reveals the DQPT driven by the defect perturbation.

The critical condition for the phase transition from dynamical polarized phase ($\langle M_z(t)\rangle \neq 0$) to dynamical non-polarized phase ($\langle M_z(t)\rangle = 0$) can be obtained according to the energy of the system.

Initially, the system is in the $k = k_0$ momentum state-the dynamical polarized state, $M_z(0) = 1$, i.e. $n_{\sigma,-} = 0$, $\varphi_{\sigma,-} = 0$, $n_{\mathrm{L},+} + n_{\mathrm{R},+} = 1$, $\varphi_\sigma = \varphi_i = 0$. The energy of the system equation (4) is reduced to

$$H(0) = 2\cos k\cos\phi + 2\Delta n_0 \sin k\sin\phi + K\sqrt{1-(\Delta n_0)^2} + \frac{g}{4}(1-(\Delta n_0)^2), \tag{6}$$

where, $\Delta n_0 = n_{\mathrm{L},+}(0) - n_{\mathrm{R},+}(0)$ is the initial atomic density difference of the $k = k_0$ quantum state between the left and right ladder legs. For the dynamical non-polarized state, $M_z(t) = 0$, the two quantum states $k = \pm k_0$ are resonantly coupled and equally occupied, i.e. $\varphi_i = 0$, $\varphi_\sigma = \pi$, $n_{\mathrm{L},+} + n_{\mathrm{R},+} = n_{\mathrm{L},-} + n_{\mathrm{R},-}$, $n_{\mathrm{L},+} - n_{\mathrm{R},+} = \Delta n_0/2$ and $n_{\mathrm{L},-} - n_{\mathrm{R},-} = -\Delta n_0/2$ are the atomic density differences of the two quantum states between the left and right ladder legs, respectively. The energy of the system becomes

$$H(M_z(t)=0) = 2\cos k\cos\phi + 2\Delta n_0 \sin k\sin\phi + K\sqrt{1-(\Delta n_0)^2} + \frac{g}{8}(1+(\Delta n_0)^2) + \frac{\varepsilon}{N}\sqrt{1-(\Delta n_0)^2}. \tag{7}$$

In order to inhibit the DQPT from the dynamical polarized state ($M_z(t) = 1$) to the dynamical non-polarized state ($M_z(t) = 0$), the initial energy should be larger than that in the dynamical non-polarized state, that is, $H(0) > H(M_z(t) = 0)$. Therefore, the critical condition for occurrence of the DQPT can be obtained

$$g/\varepsilon \leqslant (g/\varepsilon)_c = \frac{8\sqrt{1-(\Delta n_0)^2}}{N(1-3(\Delta n_0)^2)}. \tag{8}$$

In addition, using the plane wave state, $a_{j,\sigma} = a_{\sigma+}\mathrm{e}^{ik_0 j}$, as the stationary solution of equation (2) in the pure system, i.e. $\varepsilon_j = 0$, the dispersion relation of the system can be obtained

$$\begin{aligned} \mu a_{\mathrm{L}+} &= -2a_{\mathrm{L}+}\cos(k_0-\phi) - Ka_{\mathrm{R}+} + g|a_{\mathrm{L}+}|^2 a_{\mathrm{L}+} \\ \mu a_{\mathrm{R}+} &= -2a_{\mathrm{R}+}\cos(k_0+\phi) - Ka_{\mathrm{L}+} + g|a_{\mathrm{R}+}|^2 a_{\mathrm{R}+}, \end{aligned} \tag{9}$$

we can analytically obtain

$$\triangle n_0 = 2\sin k_0 \sin\phi/(g-\mu-2\cos k_0\cos\phi), \tag{10}$$

where μ is the ground state chemical potential of the system and $a_{j,\sigma}$ satisfies the normalization condition $\Sigma_j(|a_{j,\mathrm{L}}|^2 + |a_{j,\mathrm{R}}|^2) = 1$.

Equation (8) shows the competition relationship between atomic interaction g and defect ε. To confirm the DQPT predicted by equation (8), we perform numerical simulation of the discrete nonlinear Schrödinger equation $i\,\mathrm{d}a_{j,\sigma}/\mathrm{d}t = \partial H/\partial a^*_{j,\sigma}$ corresponding to equation (2) by using the fourth-order Runge–Kutta method. Initially, the system is prepared in the $k = k_0$ momentum state, which can be realized in current experiments [44, 45, 52–54]. Periodic boundary condition with $k = 2\pi l/N$ is used, $l = 0, \ldots, N-1$ is an integer, here we take $l = 1$. Then, $M_z(t)$ is calculated and DQPT is identified. Experimentally, the momentum components of the corresponding momentum eigenstate of particles can be revealed in a time-of-flight measurements [44, 45] and $M_z(t)$ can be obtained. The theoretical and numerical results are shown in figures 2 and 3, which well confirm the theoretical predications.

3.2. DQPTs

The change of $\langle M_z(t)\rangle$ and $M_z(t)$ against g/ε and t for different parameters is shown in figures 2(a) and (b), respectively. When $g/\varepsilon < (g/\varepsilon)_c$, the defect perturbation is dominate, $\langle M_z(t)\rangle = 0$, the system is in the dynamical non-polarized phase, while for $g/\varepsilon > (g/\varepsilon)_c$, the atomic interaction is dominate, $\langle M_z(t)\rangle$ suddenly jumps from $\langle M_z(t)\rangle = 0$ to $\langle M_z(t)\rangle = 1$, the system is in the dynamical polarized phase. That is, the system undergoes a DQPT when one tunes g/ε through the threshold. Figure 2(b) clearly depicts the transformation between quantum states of the system caused by defect perturbation. At the beginning ($t = 0$), the system is in the $k = k_0$ single quantum state ($M_z(0) = 1$). When $g/\varepsilon = 0.5(g/\varepsilon)_c$, $M_z(t)$ oscillates periodically between 1 and -1 with t, the defect perturbation drives the resonant coupling of the $k = k_0$ and $k = -k_0$ momentum states, the system has a periodic transformation from one polarized state ($M_z(t) = 1$) to another polarized state ($M_z(t) = -1$), and the intermediate superposition state-dynamical non-polarized state ($M_z(t) = 0$) is excited, resulting in periodic DQPT, and the system is in dynamical non-polarized phase. When $g/\varepsilon = 1.2(g/\varepsilon)_c$, $M_z(t)$ oscillates periodically between 0 and 1 with t, which indicates that atomic interaction inhibits the transformation of the condensate from $k = k_0$ single momentum state to $k = -k_0$ single momentum state. The condensate is always in the dynamical polarized state. When $g/\varepsilon = 10(g/\varepsilon)_c$, $M_z(t) \to 1$, the strong atomic interaction compensates for the effect of defect, similar to the pure system, the system remains in the initial polarized state.

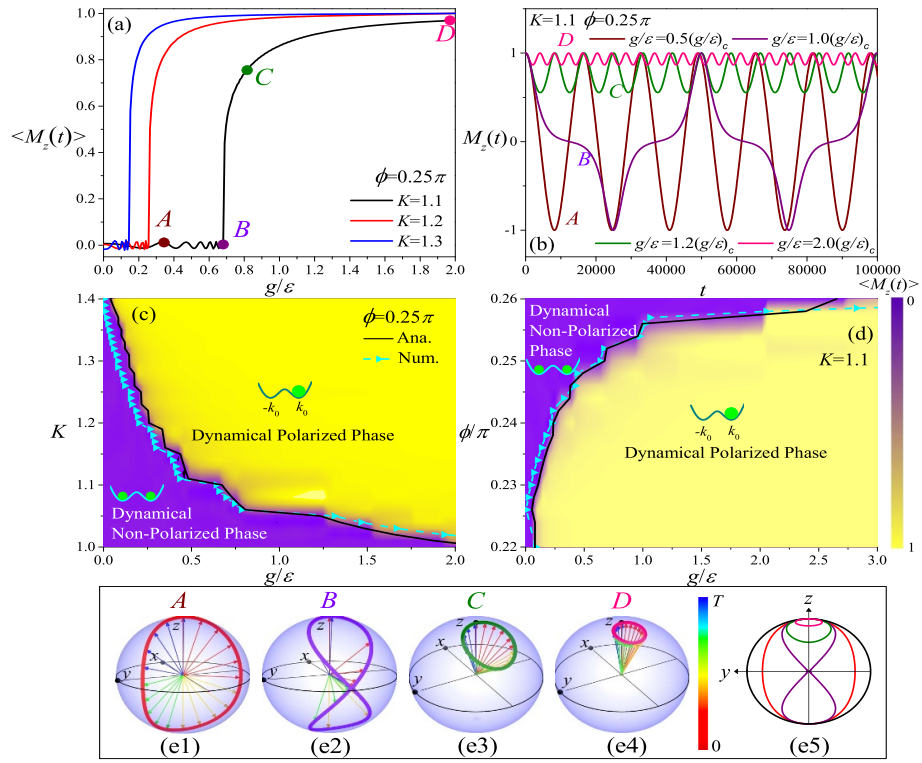

Figure 2. Dynamical phase diagram. (a) $\langle M_z(t)\rangle$ as a function of g/ε under different K. (b) $M_z(t)$ versus t for different g/ε as marked by A, B, C, and D in figure 1(a). The phase diagrams of DQPT indicated by a sharp change in $\langle M_z(t)\rangle$ in $(g/\varepsilon, K)$ (c) and $(g/\varepsilon, \phi)$ (d) planes. The color represents the magnitude of $\langle M_z(t)\rangle$. The solid lines in (c) and (d) are the analytical solution of equation (8) and the symbol lines are the numerical simulation of the equation (2). $\varepsilon = 0.01$. (e) Pseudospin evolution on the Bloch spherical surface as marked by A, B, C, and D in figure 1(a). (e1)–(e4) The arrows depict the direction of the pseudospin Bloch vector $(M_x(t), M_y(t), M_z(t))$ during a single evolution period which starts from the north point, with the color quantifying the evolution time and the colored solid line represents the evolution path. T is the oscillating period of $M_\delta(t)$. (e5) The projection of the evolution path on $y-z$ plane for different g/ε.

On varying the ratios between $K(\phi)$ and g/ε, two distinct dynamical phases emerge, for which the time-averaged polarizability ($\langle M_z(t)\rangle$) serves as an order parameter. The system features a transition from a dynamical non-polarized phase with $\langle M_z(t)\rangle = 0$ to a dynamical polarized phase with $\langle M_z(t)\rangle > 0$ at $g/\varepsilon = (g/\varepsilon)_c$. This transition is clearly indicated by the phase diagrams of the DQPT in $(g/\varepsilon, K)$ and $(g/\varepsilon, \phi)$ planes in figures 2(c) and (d). We observe abrupt changes of the order parameter $\langle M_z(t)\rangle$ at the critical point, which marks a continuous phase transition between the two dynamical phases. The phase diagram can be efficiently adjusted by parameter K and ϕ. Furthermore, in the dynamical non-polarized phase, the defect perturbation is dominate, this causes large oscillations of the instantaneous polarizability $M_z(t)$, the pseudospin Bloch vector $M_\delta(t)$ breaks through the equatorial (x-y) plane and rotates about the entire Bloch sphere, where the condensate undergoes complete transitions (figures 2(e1) and (e2)). Conversely, in the dynamical polarized phase, the atomic interaction is dominate, $M_z(t)$ oscillates about a non-zero time-averaged value, $M_\delta(t)$ evolves only within the upper half spherical surface (figures 2(e3) and (e4)). The evolution paths of $M_\delta(t)$ as marked by A, B, C, and D in figure 2(a) are clearly shown by the projection on y-z plane in figure 2(e5).

The nonequilibrium quantum dynamics is further clearly depicted in figure 3. Corresponding to figure 2(b), figure 3 shows the atomic density distributions n_σ and local current configurations at different times. At $t = 0$, the system is in the $k = k_0$ momentum state with Z_2 symmetry-broken, atoms are evenly distributed along the legs and $n_L > n_R$. The currents along the two legs are equal and opposite, the rung currents disappear. Since then, due to the defect perturbation, when $g/\varepsilon = 0.5(g/\varepsilon)_c$ (figure 3(a)), with the increase of t, corresponding to figure 2(b), the system gradually undergoes periodical transition of the dynamical fully polarized state (the $k = k_0$ momentum state with $n_L > n_R$, $t = 0$)-dynamical full non-polarized state (the vortex state with superposition of $k = k_0$ and $k = -k_0$ states, $t = T/4$)-dynamical fully polarized state (the $k = -k_0$ momentum state with $n_L < n_R$, $t = T/2$)-dynamical full non-polarized state (the vortex state, $t = 3T/4$)-dynamical fully polarized state (the $k = k_0$ momentum state with $n_L > n_R$, $t = T$), here, T is the oscillating period of $M_z(t)$. The system belongs to dynamical non-polarized phase, i.e. $\langle M_z(t)\rangle = 0$. When $g/\varepsilon = 1.2(g/\varepsilon)_c$ (figure 3(b)), the polarized state with $k = -k_0$ can not be excited, a large

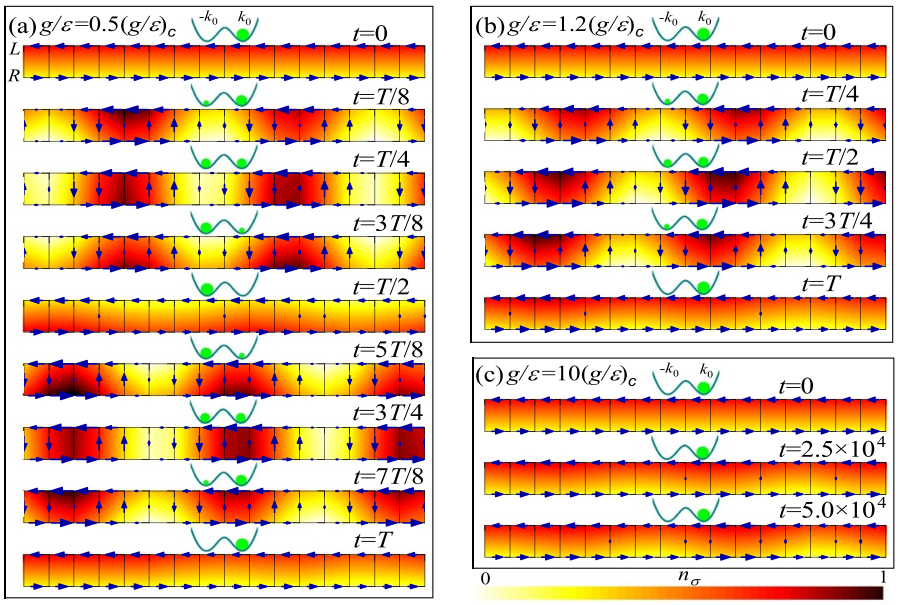

Figure 3. Temporal evolution of patterns of atomic density distributions and local current configurations with different g/ε. $K=1.1$, $\phi=0.25\pi$, $\varepsilon=0.01$.

g inhibits the DQPT and the system is in the dynamical polarized phase, i.e. $\langle M_z(t)\rangle > 0$. When $g/\varepsilon = 10(g/\varepsilon)_c$ (figure 3(c)), $M_z(t)\to 1$, the sufficiently larger g compensates the effect of the defect, and the system keeps in the dynamical fully polarized state.

Interestingly, in dynamical non-polarized phase, due to the resonant coupling of the two single quantum states with $k=k_0$ ($n_\mathrm{L} > n_\mathrm{R}$) and $k=-k_0$ ($n_\mathrm{L} < n_\mathrm{R}$), we clearly observe the periodic appearance and annihilation of dynamical vortex and the manifestation of symmetry restoration (the vortex state) after perturbation from broken-symmetry phase, this temporal evolution of patterns of atomic density distributions and local current configurations is deeply related to the underlying ground state phase diagram and can be used to approximately capture the DQPT. Therefore, a thorough connection among the order parameter dynamics, the underline ground state phase transition and nonequilibrium dynamics is established in real time and real space.

3.3. Probing the underlying ground state phase by quenching the defect

Importantly, the connection between the nonequilibrium dynamics and the underlying ground state phases shown in figure 3(a) may pave a new way to study the underlying complex ground state phases and can be used to observe the ground states which are often experimentally challenging to reach. Here, we can easily capture the different ground state phases of the system through quenching the defect at certain time, so as to identify and control them. Figure 4(a) shows quenching the defect at $t=T/2$, $t=3T/4$ and $t=T$ in the dynamical process. When $t=T/2$ and $t=T$, the system is in the $k=-k_0$ ($M_z(t)=-1$) or $k=k_0$ ($M_z(t)=1$) momentum state. When the defect is suddenly removed at these times, the system stably maintains the underlying dynamical polarized state, i.e. $M_z(t)\equiv -1$ or $M_z(t)\equiv 1$. Figure 4(b) further demonstrates that, until $t=50\,000\approx 2.5T$ after quenching the defect, atoms are evenly distributed along the legs ($n_\mathrm{L} > n_\mathrm{R}$ for $M_z(t)=1$ and $n_\mathrm{L} < n_\mathrm{R}$ for $M_z(t)=-1$), the rung currents disappear, the system maintains the $k=k_0$ or $k=-k_0$ momentum state. That is, the stable BL phase is maintained. In addition, when $t=3T/4$, the system is in the dynamical fully non-polarized state with superimposed two momentum states. When the defect is suddenly removed at this time, $M_z(t)\equiv 0$ and does not change with t, even at $t=50\,000\approx 2.5T$ after the quenching (see figure 4(b)), the system remains in the vortex phase. The ground state phases of the system can be identified by quenching the defect, which provides a feasible dynamical measurement scheme for observing the BL phase in the experiment.

4. The DQPT induced by the random defects perturbation

Now we discuss the nonequilibrium quantum dynamics of the system induced by the random defects perturbation numerically. ε_n is a random uncorrelated on site potential taken to be uniformly distributed, $\varepsilon_n\in[0,\bar{\varepsilon}]$. We have taken the average value $\overline{M_z(t)}$ of $M_z(t)$ for multiple evolutions

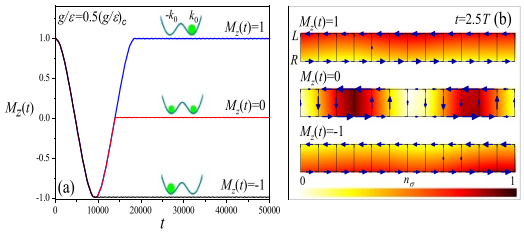

Figure 4. (a) $M_z(t)$ versus t when the defect is quenched at $t = T/2$, $t = 3T/4$ and $t = T$ in the dynamical non-polarized phase. (b) Patterns of atomic density distributions and local current configurations until $t = 50\,000 \approx 2.5T$ after quenching the defect. $K = 1.1$, $g/\varepsilon = 0.5(g/\varepsilon)_c$, $\phi = 0.25\pi$, $\varepsilon = 0.01$.

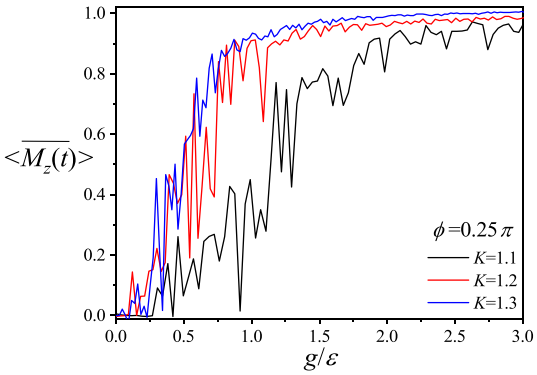

Figure 5. $\langle\overline{M_z(t)}\rangle$ as a function of g/ε under different K. $\bar{\varepsilon} = 0.01$, $\phi = 0.25\pi$.

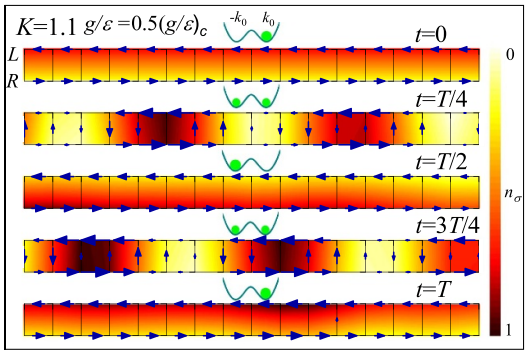

Figure 6. Patterns of atomic density distributions and local current configurations at different t. $K = 1.1$, $\phi = 0.25\pi$, $\bar{\varepsilon} = 0.01$.

(here we take ten evolutions as samples) as the order parameter to distinguish the quantum states, i.e. $\langle\overline{M_z(t)}\rangle = \langle\sum_i^{10} M_{zi}(t)/10\rangle$.

When the initial state is in the single momentum state, as shown in figure 5, the change of the order parameter $\langle\overline{M_z(t)}\rangle$ is similar to that of the single defect system, so the effect of the random defects on dynamical phase transition is similar to an effective single defect. Similar to the previous research results, the system has a critical value $(g/\varepsilon)_c$, when $g/\varepsilon < (g/\varepsilon)_c$, the random defects perturbation leads to the resonant coupling between the two quantum states, $\langle\overline{M_z(t)}\rangle \to 0$, the system is in the dynamical non-polarized phase. When $g/\varepsilon > (g/\varepsilon)_c$, $\langle\overline{M_z(t)}\rangle \to 1$, g inhibits the resonant coupling effect and the system is in the dynamical polarized phase. In addition, the change of $\langle\overline{M_z(t)}\rangle$ is much more complex than that with the single lattice defect near the threshold, and greater g is needed to compensate the effect of defects on the system, which further reflects the complexity of the random defects system.

Figure 6 shows the nonequilibrium quantum dynamics induced by the random defects perturbation. Consistent with the single defect system, with the increase of t, the system undergoes the dynamical fully polarized state (the $k = k_0$ quantum state, $t = 0$)-dynamical fully non-polarized state (the vortex state, $t = T/4$)-dynamical fully polarized state (the $k = -k_0$ quantum state, $t = T/2$)-dynamical fully non-polarized state (the vortex state, $t = 3T/4$)-dynamical fully polarized state (the $k = k_0$ quantum state,

$t = T$) quantum phase transition. The quantum phase transition from the dynamical polarized state (the BL phase) to the dynamical non-polarized state (the vortex phase) is excited, the random defects perturbation can also make the system undergo DQPT.

5. Conclusion

In summary, we report on the first prediction of DQPT in a magnetized interacting Bose–Hubbard flux ladder induced by defect perturbation. The DQPT is demonstrated by the observable order parameter and the temporal evolution of patterns of atomic density distributions and local current configurations. A clear correspondence between the DQPT and underlying ground state phase transition is established, which makes us to identify and capture the ground state phase by quenching the defect. This work elaborates the potential mechanism of the quantum state transition caused by defect perturbation, which provides an important way to study the nonequilibrium quantum dynamics in the optical lattice with atomic interaction. Our methodology can be applied in a much more general context, and open new possibilities for the study of DQPT, ground state phases and many-body localization phenomena of atomic gases in optical lattices beyond one dimension.

Data availability statement

All data that support the findings of this study are included within the article (and any supplementary files).

Acknowledgments

This work is supported by the National Natural Science Foundation of China under Grants No. 12164042, 12264045, 12104374, 11764039 and 11847304, and by Innovation capability enhancement project of Gansu higher education under Grand No. 2020A-146.

ORCID iDs

Zi-Fa Yu https://orcid.org/0000-0001-5012-0148
Ju-Kui Xue https://orcid.org/0000-0001-7854-5869

References

[1] Polkovnikov A, Sengupta K, Silva A and Vengalattore M 2011 *Rev. Mod. Phys.* **83** 863
[2] Eisert J, Friesdorf M and Gogolin C 2015 *Nat. Phys.* **11** 124
[3] Heyl M 2018 *Rep. Prog. Phys.* **81** 054001
[4] Zvyagin A A 2016 *Low Temp. Phys.* **42** 971
[5] Chen Z, Tang T, Austin J, Shaw Z, Zhao L and Liu Y 2019 *Phys. Rev. Lett.* **123** 113002
[6] Liu B and Hu J 2015 *Phys. Rev.* A **92** 013606
[7] Sun W *et al* 2018 *Phys. Rev. Lett.* **121** 250403
[8] Yang H X, Tian T, Yang Y B, Qiu L Y, Liang H Y, Chu A J, Dag C B, Xu Y, Liu Y and Duan L M 2019 *Phys. Rev.* A **100** 013622
[9] Smale S, He P, Olsen B A, Jackson K G, Sharum H, Trotzky S, Marino J, Rey A M and Thywissen J H 2019 *Sci. Adv.* **5** eaax1568
[10] Fläschner N, Vogel D, Tarnowski M, Rem B S, Lühmann D-S, Heyl M, Budich J C, Mathey L, Sengstock K and Weitenberg C 2018 *Nat. Phys.* **14** 265
[11] Heyl M 2014 *Phys. Rev. Lett.* **113** 205701
[12] Muniz J A, Barberena D, Lewis-Swan R J, Young D J, Cline J R K, Rey A M and Thompson J K 2020 *Nature* **580** 602
[13] Jurcevic P, Shen H, Hauke P, Maier C, Brydges T, Hempel C, Lanyon B P, Heyl M, Blatt R and Roos C F 2017 *Phys. Rev. Lett.* **119** 080501
[14] Zhang J, Pagano G, Hess P W, Kyprianidis A, Becker P, Kaplan H, Gorshkov A V, Gong Z X and Monroe C 2017 *Nature* **551** 601
[15] Xu K *et al* 2020 *Sci. Adv.* **6** eaba4935
[16] Nalbach P and Thorwart M 2013 *Phys. Rev.* B **87** 014116
[17] Otterpohl F , Nalbach P and Thorwart M 2022 *Phys. Rev. Lett.* **129** 120406
[18] Wang Q, Hu A Y and Zheng H 2009 *Phys. Rev.* B **80** 214301
[19] Kast D and Ankerhold J 2013 *Phys. Rev. Lett.* **110** 010402
[20] Tian T, Yang H X, Qiu L Y, Liang H Y, Yang Y B, Xu Y and Duan L M 2020 *Phys. Rev. Lett.* **124** 043001
[21] Halimeh J C, Zauner-Stauber V, McCulloch I P, de Vega I, Schollwöck U and Kastner M 2017 *Phys. Rev.* B **95** 024302
[22] Mori T, Ikeda T N, Kaminishi E and Ueda M 2018 *J. Phys. B: At. Mol. Opt. Phys.* **51** 112001
[23] De Nicola S, Michailidis A A and Serbyn M 2021 *Phys. Rev. Lett.* **126** 040602
[24] Poon T F J and Liu X J 2016 *Phys. Rev.* A **93** 063420
[25] Bando Y and Nishimori H 2021 *Phys. Rev.* A **104** 022607
[26] Kim S P and Lee C H 2000 *Phys. Rev.* D **62** 125020
[27] Liang S, Wang Z W, Qin J, Zhao X D and Zhou L 2021 *Results Phys.* **29** 104678
[28] Bhattacharya U, Bandyopadhyay S and Dutta A 2017 *Phys. Rev.* B **96** 180303(R)
[29] Bhattacharya U and Dutta A 2017 *Phys. Rev.* B **96** 014302
[30] Heyl M and Budich J C 2017 *Phys. Rev.* B **96** 180304(R)

[31] Heyl M 2015 *Phys. Rev. Lett.* **115** 140602
[32] Karrasch C and Schuricht D 2017 *Phys. Rev.* B **95** 075143
[33] DeNicola S, Michailidis A A and Serbyn M 2021 *Phys. Rev. Lett.* **126** 040602
[34] Zhou B, Zeng Y and Chen S 2021 *Phys. Rev.* B **104** 094311
[35] Lang H, Chen Y, Hong Q and Fan H 2018 *Phys. Rev.* B **98** 134310
[36] Heyl M, Polkovnikov A and Kehrein S 2013 *Phys. Rev. Lett.* **110** 135704
[37] Kennes D M, Schuricht D and Karrasch C 2018 *Phys. Rev.* B **97** 184302
[38] Abdi M 2019 *Phys. Rev.* B **100** 184310
[39] Syed M, Enss T and Defenu N 2021 *Phys. Rev.* B **103** 064306
[40] Fogarty T, Usui A, Busch T, Silva A and Goold J 2017 *New J. Phys.* **19** 113018
[41] Homrighausen I, Abeling N O, Zauner-Stauber V and Halimeh J C 2017 *Phys. Rev.* B **96** 104436
[42] Halimeh J C and Zauner-Stauber V 2017 *Phys. Rev.* B **96** 134427
[43] Žunkovič B, Heyl M, Knap M and Silva A 2018 *Phys. Rev. Lett.* **120** 130601
[44] Atala M, Aidelsburger M, Lohse M, Barreiro J T, Paredes B and Bloch I 2014 *Nat. Phys.* **10** 588
[45] Hügel D and Paredes Ben 2014 *Phys. Rev.* A **89** 023619
[46] Greschner S, Filippone M and Giamarchi T 2019 *Phys. Rev. Lett.* **122** 083402
[47] Richaud A, Ferraretto M and Capone M 2021 *Phys. Rev.* B **103** 205132
[48] Orignac E and Giamarchi T 2001 *Phys. Rev.* B **64** 144515
[49] Piraud M, Heidrich-Meisner F, McCulloch I P, Greschner S, Vekua T and Schollwöck U 2015 *Phys. Rev.* B **91** 140406(R)
[50] Di Dio M, Citro R, De Palo S, Orignac E and Chiofalo M-L 2015 *Eur. Phys. J. Spec. Top.* **224** 525
[51] Greschner S and Vekua T 2017 *Phys. Rev. Lett.* **119** 073401
[52] Greschner S, Piraud M, Heidrich-Meisner F, McCulloch I P, Schollwöck U and Vekua T 2016 *Phys. Rev.* A **94** 063628
[53] Wei R and Mueller E J 2014 *Phys. Rev.* A **89** 063617
[54] Buser M, Hubig C, Schollwöck U, Tarruell L and Heidrich-Meisner F 2020 *Phys. Rev.* A **102** 053314
[55] Uchino S and Tokuno A 2015 *Phys. Rev.* A **92** 013625
[56] Tschischik W, Haque M and Moessner R 2012 *Phys. Rev.* A **86** 063633
[57] Zheng Y, Feng S and Yang S J 2017 *Phys. Rev.* A **96** 063613
[58] Li Z H, Zhou L and Li Y 2021 *J. Phys.* B **54** 035004
[59] Liang S, Li Z C, Zhang W P, Zhou L and Lan Z H 2020 *Phys. Rev.* A **102** 033332
[60] Zhang A X, Cai L X, He S Q, Yu Z F, Qiao X, Zhang Y and Xue J K 2019 *Europhys. Lett.* **127** 50007
[61] Zhao Y J, Tan N, Yu D, Liu B and Liu W M 2020 *Phys. Rev. Res.* **2** 033484
[62] Tschischik W, Moessner R and Haque M 2015 *Phys. Rev.* A **92** 023845
[63] Qiao X, Zhang X B, Jian Y, Zhang A X, Yu Z F and Xue J K 2021 *Phys. Rev.* A **104** 053323
[64] Jian Y, Qiao X, Liang J C, Yu Z F, Zhang A X and Xue J K 2021 *Phys. Rev.* E **104** 024212
[65] Suthar K, Sierant P and Zakrzewski J 2020 *Phys. Rev.* B **101** 134203
[66] Carrasquilla J, Becca F and Fabrizio M 2011 *Phys. Rev.* B **83** 245101
[67] White M, Pasienski M, McKay D, Zhou S Q, Ceperley D and DeMarco B 2009 *Phys. Rev. Lett.* **102** 055301
[68] Gavish U and Castin Y 2005 *Phys. Rev. Lett.* **95** 020401
[69] Gimperlein H, Wessel S, Schmiedmayer J and Santos L 2005 *Phys. Rev. Lett.* **95** 170401
[70] Gati R and Oberthaler M K 2007 *J. Phys.* B **40** R61
[71] Pigneur M and Schmiedmayer J 2018 *Phys. Rev.* A **98** 063632
[72] Trombettoni A, Smerzi A and Bishop A R 2002 *Phys. Rev. Lett.* **88** 173902